Author/s:
Zhong, Q;Richardson, JJ;Li, S;Zhang, W;Ju, Y;Li, J;Pan, S;Chen, J;Caruso, F

Title:
Expanding the Toolbox of Metal–Phenolic Networks via Enzyme‐Mediated Assembly

Date:
2020-01-20

Citation:
Zhong, Q., Richardson, J. J., Li, S., Zhang, W., Ju, Y., Li, J., Pan, S., Chen, J. & Caruso, F. (2020). Expanding the Toolbox of Metal–Phenolic Networks via Enzyme‐Mediated Assembly. Angewandte Chemie, 132 (4), pp.1728-1734. https://doi.org/10.1002/ange.201913509.

Title: Expanding the Toolbox of Metal–Phenolic Networks via Enzyme-Mediated Assembly

Authors: Qi-Zhi Zhong; Joseph J. Richardson; Shiyao Li; Wenjie Zhang; Yi Ju; Jianhua Li; Shuaijun Pan; Jingqu Chen; Frank Caruso, Prof.

To be cited as: 10.1002/ange.201913509

Link to VoR: https://doi.org/10.1002/ange.201913509

Expanding the Toolbox of Metal–Phenolic Networks via Enzyme-Mediated Assembly

Qi-Zhi Zhong, Joseph J. Richardson, Shiyao Li, Wenjie Zhang, Yi Ju, Jianhua Li, Shuaijun Pan, Jingqu Chen, and Frank Caruso*

Abstract: Functional coatings are of considerable interest because of their fundamental implications for interfacial assembly and promise for numerous applications. Universally adherent materials have recently emerged as versatile tools to engineer functional coatings; however, such coatings are generally limited to catechol, (*ortho*-diphenol)-containing molecules, as building blocks. Here, we report a facile, biofriendly enzyme-mediated strategy for assembling a wide range of molecules (e.g., 14 representative molecules in this study) that do not natively have catechol moieties, including small molecules, peptides, and proteins, on various surfaces, while preserving the molecule's inherent function, such as catalysis (~80% retention of enzymatic activity for trypsin). Assembly is achieved by in situ conversion of monophenols into catechols via tyrosinase, where films form on surfaces via covalent and coordination cross-linking. The resulting coatings are robust, functional (e.g., in protective coatings, biological imaging, and enzymatic catalysis), and versatile for diverse secondary surface-confined reactions (e.g., biomineralization, metal ion chelation, and *N*-hydoxysuccinimide conjugation).

Advances in designing functional materials are highly dependent on the development of surface modification strategies,[1] which can significantly change the interfacial properties of a material (e.g., morphology, wettability, and degradability)[2] and thus govern its performance in specific applications, including drug delivery,[3] catalysis,[4] biological imaging,[5] and energy storage.[6] Recently, phenolic compounds have garnered significant interest as building blocks for the assembly of functional coatings and films owing to their desirable properties including versatile adhesion,[7] selective permeability,[8] high antioxidation,[9] and excellent stability.[10] For example, Lee et al. reported organic polydopamine (PDA) coatings,[11] and our group reported hybrid metal–phenolic networks (MPNs),[12] both of which are useful for coating various surfaces with different size, shape, structure, and composition.[7b,13] Such versatile adhesion between the phenolic molecules (e.g., dopamine and tannic acid) and substrates is believed to derive from the diverse interfacial interactions generated by catechol moieties in the precursors.[14] Therefore, the phenolic building blocks reported to date almost all have at least one catechol group.[15] However, overcoming the constraints of the catechol-specific thin film toolbox is expected to provide greater versatility and functionality for surface modification. Considering the functionality of phenolic compounds and their ubiquitous presence in nature,[16] a facile method capable of converting arbitrary phenolic molecules into thin film building blocks could be a promising strategy to expand the "phenolic coating" toolbox.

We herein present a facile enzyme-mediated strategy for assembling diverse monophenol-based molecules on various surfaces to engineer a range of coatings, films, and particles. Specifically, assembly is achieved by two steps (Scheme 1a), where the monophenol group of the studied molecule (precursor molecule) is first converted into a catechol moiety by tyrosinase (Scheme 1b), which is an efficient enzyme widely used in nature to synthesize catechol-containing molecules such as melanin and mussel adhesive proteins.[17] This conversion is then followed by molecular assembly on a given substrate surface directed by the energetic adhesion between the catechol moieties and the substrate and cross-linking via covalent and coordination bonding (Scheme 1c,d). This strategy enables the assembly of 14 representative monophenol-based molecules, ranging from small molecules to proteins, on surfaces. Importantly, the enzymatic hydroxylation and subsequent reactions are mild and efficient, thereby preserving the functionality of the precursor molecules, including enzymatic catalysis (e.g., ~80% retention of enzymatic activity for trypsin after deposition), radical scavenging, fluorescence, and cell compatibility. Our study greatly expands the toolbox of materials useful for synthesizing versatile coatings/films and has fundamental implications for the interfacial chemistry of phenolic assembly. From a fundamental perspective, monophenols are the most basic phenolic group, and strategies for assembling monophenol-based molecules have significant implications for materials design such as for metal–phenolic networks, universal coatings, and underwater adhesives.

We first describe the formation of films from tyrosine, an amino acid with a monophenol side group (Figure 1a), on planar and particle substrates. After the addition of tyrosinase, the tyrosine solution gradually turned orange. UV–Visible (UV–vis) spectroscopy analysis (Figure 1d) showed peaks at 310 nm (quinone peak) and 480 nm (cyclic amine peak) after reacting for 2 h, indicating the hydroxylation of tyrosine to 3,4-dihydroxyphenylalanine (DOPA) by tyrosinase, which can be further oxidized to DOPA-quinone, DOPA-chrome, and DOPA-polymer (Figure 1c).[18] We then added $FeCl_2$ to the tyrosine derivative (e.g., DOPA, DOPA-quinone, DOPA-chrome, and DOPA-polymer, denoted as tyrosine′) solution, which rapidly turned black–green (Figure 1b). The UV–vis absorbance peak observed at 650 nm (Figure 1e) can be attributed to the characteristic ligand-to-metal charge transfer (LMCT) band of catechol moieties interacting with iron ions, suggesting the occurrence of coordination bonds in solution.[15c] After incubation with $FeCl_2$ for 1 h, the coated substrates (i.e., glass slides, polystyrene (PS) particles, and stainless steel mesh) turned brown–black (Figure S1, Supporting Information), and scanning electron microscopy (SEM; Figure 1g,h and Figure S2) confirmed the formation of a coating. After removing the PS

Q.-Z. Zhong, Dr. J. J. Richardson, S. Li, Dr. W. Zhang, Dr. Y. Ju, Dr. J. Li, Dr. S. Pan, J. Chen, Prof. F. Caruso
ARC Centre of Excellence in Convergent Bio-Nano Science and Technology, and the Department of Chemical Engineering, The University of Melbourne, Parkville, Victoria 3010, Australia
Email: fcaruso@unimelb.edu.au

Supporting information for this article is given via a link at the end of the document.

particles, free-

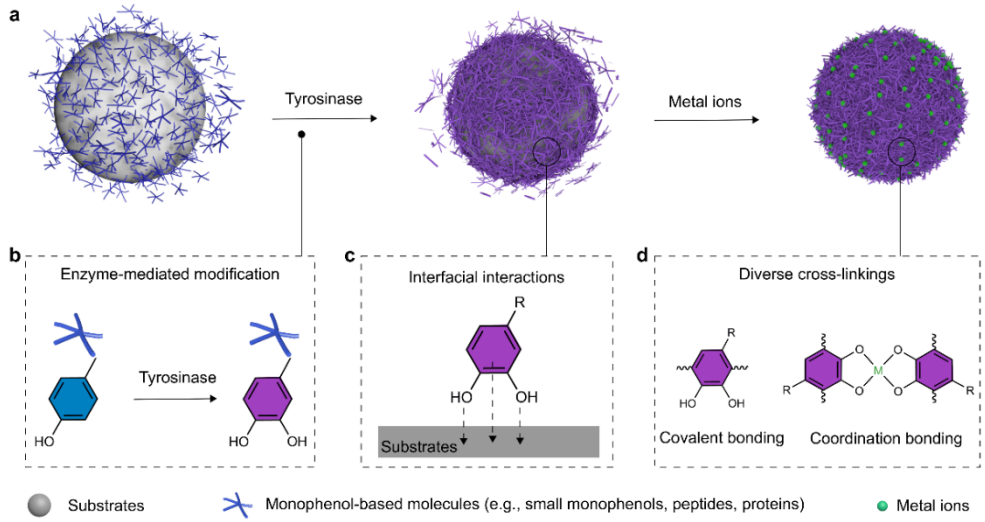

Scheme 1. (a) Schematic illustration of enzyme-mediated monophenol-based molecular assembly on a surface. (b) Enzyme-mediated conversion of a monophenol moiety into a catechol moiety. (c) Assembly of the modified molecules on a surface by diverse interfacial interactions between catechol moieties and substrates. (d) Molecular structures showing the possible routes of covalent and coordination cross-linking in the coatings.

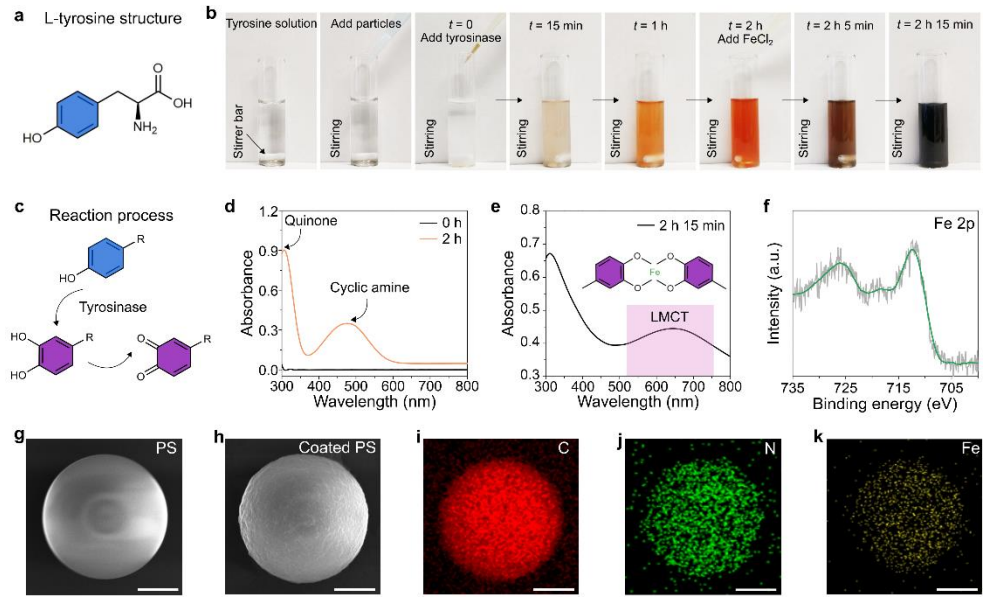

Figure 1. Formation of tyrosine′–iron films on particle substrates by enzyme-mediated assembly. (a) Molecular structure of L-tyrosine. (b) Photographs of the enzyme-mediated assembly process. (c) Schematic of the conversion of a monophenol moiety into catechol and quinone moieties by tyrosinase. (d) Conversion kinetics as monitored by UV–vis absorption spectroscopy. (e) UV–vis absorption spectrum showing the LMCT band of an iron–catechol complex, schematically shown in the inset. (f) XPS spectrum showing the presence of Fe^{III} in the tyrosine′–iron films. (g,h) SEM images of PS particles before and after tyrosine′–iron coating, and (i–k) the corresponding EDS images showing C, N, and Fe elements in the films. Scale bars, 1 μm.

standing hollow capsules of tyrosine′–iron can be obtained (Figure S3), demonstrating the formation of thin films. X-ray photoelectron spectroscopy (XPS; Figure 1f) and energy-dispersive X-ray spectroscopy (EDS; Figure 1i–k) suggest that iron in the coatings was primarily present as Fe^{III} owing to the presence of the Fe 2p peaks at binding energies of ~726 and 712 eV [19] and the distribution of element iron in the coatings. The oxidation of Fe^{II} to Fe^{III} was likely caused by the oxidation of the catechol groups in the presence of dissolved air, which is observed in other metal–phenolic complexes.[8a,19,20] Fourier transform infrared spectroscopy measurements (Figure S4) showed the stretching vibration of C–N bonds at 1630 cm^{-1},

indicating the successful coating of tyrosine-based molecules (e.g., DOPA) on the substrates, and the bands at 1557 and 1489 cm^{-1} confirmed the formation of iron–catechol complexes in the coatings.[21] To further verify that the coatings primarily comprised tyrosine′, rather than being composed of tyrosinase, the latter molecule was covalently immobilized on silica particles that were then used to trigger the hydroxylation of tyrosine. This immobilization prevented the tyrosinase from existing as a free molecule in solution, and thereby from being incorporated. The immobilized tyrosinase catalyzed the conversion of tyrosine, leading to formation of the coating (Figure S5), suggesting that the converted tyrosine itself was incorporated. In addition, the absence of a Cu 2p signal (from tyrosinase) in the XPS spectra confirmed that the amount of tyrosinase in the tyrosine′–iron coatings was negligible (Figure S6).[22] Control experiments showed that pristine tyrosine or tyrosine and $FeCl_3$, despite the oxidative properties of Fe^{III}, did not form coatings on substrates in the absence of tyrosinase (Figure S7), confirming the importance of the enzymatic conversion of the monophenol residue into catechol. Collectively, these results demonstrate that tyrosinase can trigger the conversion of monophenol groups into catechol moieties in tyrosine, which can then interact with iron ions and form coatings on various substrates. Notably, not only Fe^{II} (3d block), but other metals, including Zn^{II}, Cu^{II} (3d block), Al^{III} (3p block), and Zr^{IV} (4d block), can form tyrosine′-metal films on surfaces (Figure S8).

To further understand the formation process and the structure of the tyrosine′–metal films prepared via enzyme-mediated assembly, the growth kinetics and the stability of the films were investigated. A two-stage process was involved, where first a covalently cross-linked film was being deposited, followed by coordination-driven film growth. After incubating tyrosine with tyrosinase for 2 h (stage I) in the presence of a glass substrate, tyrosine′ films with a thickness of ~5.6 nm formed (Figure 2a,b). These films were stable in aqueous solutions at pH 1 but unstable at pH 13 (Figure S9). At stage I, the monophenol group of tyrosine is converted into a catechol moiety, eventually oxidizes to DOPA and concurrently deposits onto the substrate and polymerizes into PDA.[23] Owing to the properties of PDA, films formed at this stage are stable in acidic solutions but unstable in alkaline solutions.[24] After the addition of $FeCl_2$ to the solution (stage II), the coordination reactions occurred rapidly, and the tyrosine′–iron complexes formed (Figure S10) and subsequently deposited onto the substrate surface, resulting in an increase in the film thickness to ~16.8 nm after only 1 h (Figure 2a and c). An LMCT band was observed for the resulting films (Figure S11), suggesting the formation of iron–catechol complexes during stage II. The addition of $FeCl_2$ can both enhance the catalytic performance of tyrosinase by promoting hydroxylation of tyrosine[25] and provide iron ions to chelate catechol-containing molecules in solution.[26] This is confirmed by the control experiments, which demonstrated that the film formed after incubation for 3 h solely with tyrosinase in the absence of $FeCl_2$ has a thickness of ~12.1 nm. These iron–catechol complexes can subsequently bind to the PDA-like film, forming tyrosine′–iron networks (i.e., MPNs) on top of the PDA-like layer (Figure 2d). This binding force was sufficiently strong to even enable the formation of superstructured particles (i.e., core–satellite superparticles, Figure S12). In addition, the film thickness could be controlled by changing the concentration of the film precursors (Figure S13). The films formed in stage II were stable within pH 5–9 (Figure 2e). However, when the pH was reduced to 1, the thickness decreased to ~4 nm (a similar value obtained in stage I) and the LMCT band disappeared (Figure S11), indicating disassembly of the iron–catechol complexes in acidic solutions and a return to the covalently stabilized films formed in stage I. This is due to the protonation of the catechol moieties, which caused disassembly of the MPNs in acidic environments. Moreover, the instability of the PDA-like layer in alkaline solutions leads to the complete disassembly of the tyrosine′–iron film at pH 13 (Figure 2e and Figure S11), as it is the intermediate layer between the substrate and the MPN layer. From these observations, it is proposed that the resulting tyrosine′–iron films comprise a double-layer structure (Figure 2d). The first layer (attached to the substrate) is a PDA-like film cross-linked by covalent bonding and is stable across a wide pH range up to ~13. The second layer is an MPN film formed by the coordination of iron ions with catechol groups.

Figure 2. Growth and stability of tyrosine′–iron films on planar substrates. (a) Film growth over time at the two stages. Insets are photographs of the tyrosine′-based films on glass at different times. The scale bar in all insets is 0.5 cm. (b,c) AFM images of tyrosine′ (b) and tyrosine′–iron (c) films prepared at different incubation times. Scratches were made to measure the film thickness. Scale bars, 1 μm. (d) Schematic of tyrosine′–iron films formed by enzyme-mediated

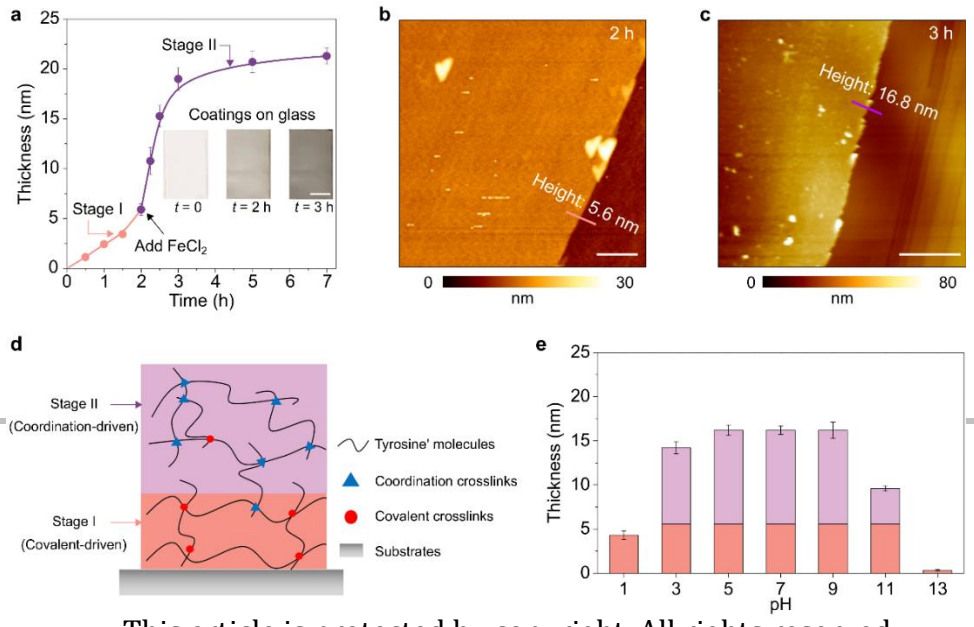

assembly, showing the double-layer film structure. (e) Thickness of the tyrosine'–iron films after incubation for 4 h in aqueous solutions at different pH.

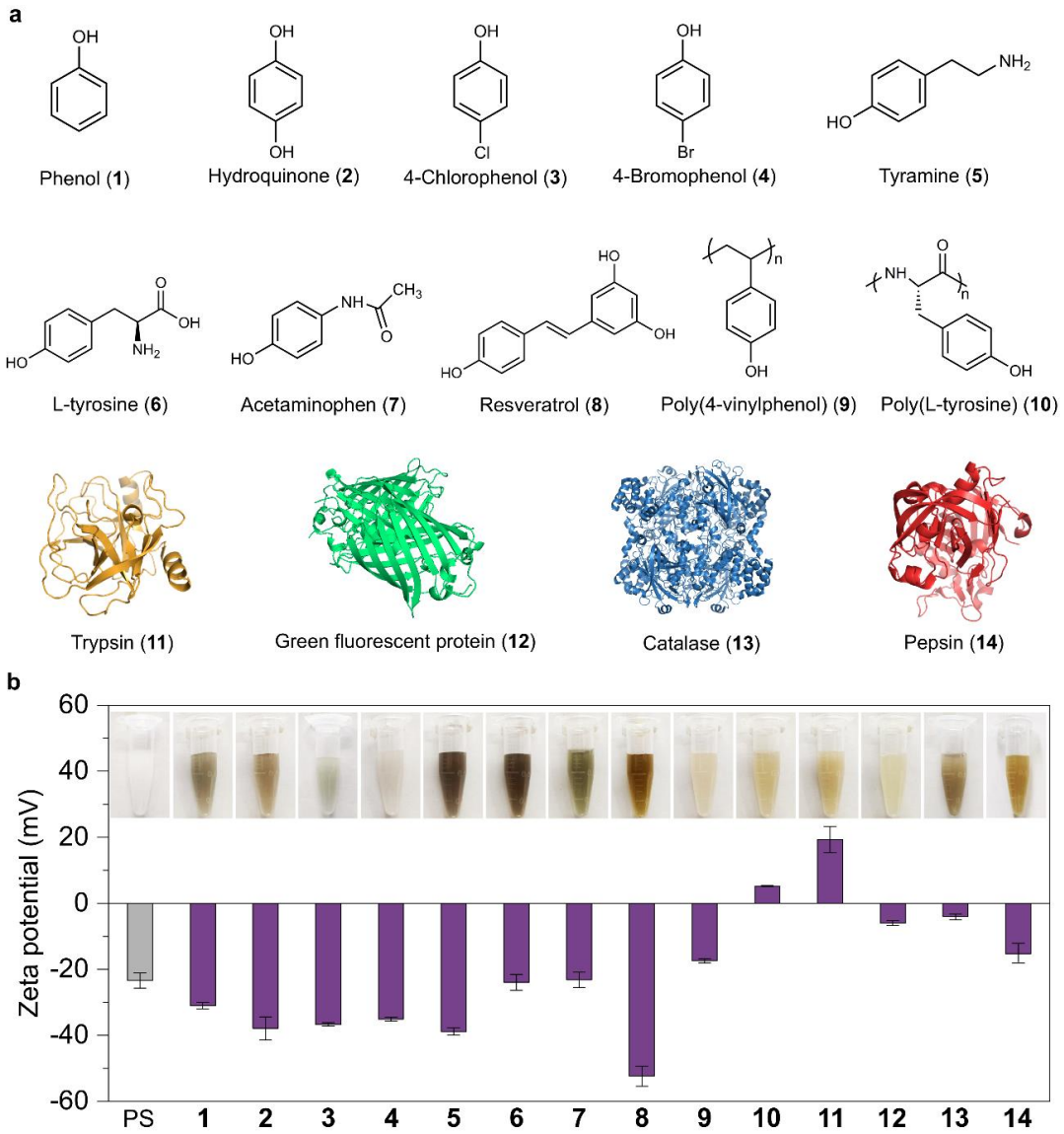

Figure 3. Assembly of various monophenol-based molecules on PS particles by enzyme-mediated assembly. (a) Molecular and schematic structures of the investigated molecules, ranging from small molecules to proteins. (b) Zeta potential values of PS particles in water before (grey) and after (purple) coating with the different molecules. The numbers on the *x*-axis correspond to the numbers used for denoting the molecules in (a). Insets are photographs of the corresponding particle suspensions.

To examine the applicability of our strategy to different monophenol-based molecules, a wide range of compounds were used to coat various substrates (Figure 3a), including small monophenols (phenol, hydroquinone, 4-chlorophenol, 4-bromophenol, tyramine, L-tyrosine, acetaminophen, and resveratrol (Res)), synthetic polymers (poly(4-vinylphenol)), peptides (poly(L-tyrosine)), and proteins (trypsin, green fluorescent protein (GFP), catalase (Cat), and pepsin). The color of the solutions of all monophenol-containing molecules studied changed after incubation with tyrosinase for 2 h (Figure S14), and the UV–vis spectra of the solutions featured new absorbance peaks after incubation with $FeCl_2$, suggesting interactions between catechol moieties and iron ions (Figure S15). The zeta potential of the PS particles changed after coating with the various molecules (Figure 3b), and SEM images (Figures 4 and S16) further confirmed the formation of coatings. Although control experiments without tyrosinase demonstrated that the nonspecific adsorption of proteins (i.e., trypsin, GFP, Cat, and pepsin) on the PS surface was negligible (Figure S17), the diverse interactions (e.g., hydrogen boding and coordination) that proteins can undergo may also slightly contribute to the formation of protein–protein or protein–metal assemblies in solution and in the coatings. It is worth noting that the monophenol groups in amine-free phenolic compounds (e.g.,

Res) can be converted into catechols by tyrosinase; however, in the absence of coordination-driven assembly, the films were very thin (Figure S18), highlighting the importance of metal chelation for promoting film formation in catechol-based amine-free systems.[27]

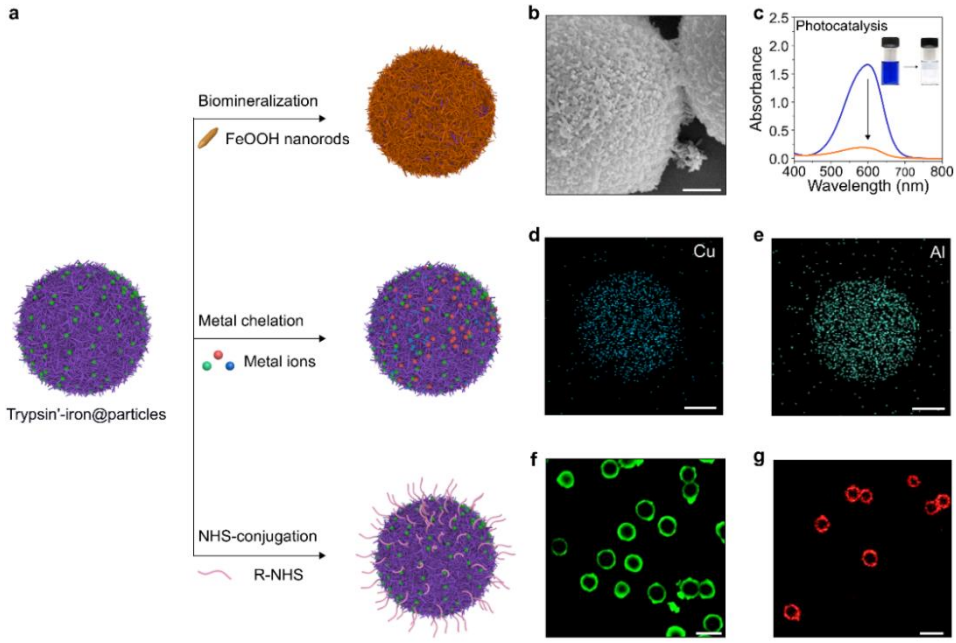

Figure 4. Trypsin′–iron coatings serve as a chemically reactive platform for secondary, surface-confined reactions. (a) Schematic illustration of different possible reactions with trypsin′–iron coatings, including biomineralization, metal chelation, and covalent conjugation using NHS-containing molecules. (b) FeOOH nanorods on trypsin′–iron-coated particles. Scale bar, 500 nm. (c) UV–vis spectra of methyl blue solution before and after the treatment with FeOOH-conjugated particles. (d,e) EDS images of trypsin′–iron-coated particles after chelating Cu and Al ions. Scale bars, 1 μm. (f,g) CLSM images of trypsin′–iron-coated particles conjugated with Alexa Fluor™ 488 (f) or 633 (g) NHS ester. Scale bars, 5 μm.

To explore the applicability of this method to deposit macromolecules on different substrates, trypsin was used to coat different nano- and microparticles. SEM (Figure S19) and zeta potential (Figure S20) analyses demonstrated that enzyme-mediated assembly could be used to form trypsin coatings on substrates with different sizes (i.e., diameter = 4.96 μm, 2.79 μm, and 580 nm), surface properties (anionic, neutral, and cationic), and compositions (inorganic and organic). After removing the core, trypsin′–iron capsules (hollow particles) with a film thickness of ~17.2 nm were obtained (Figure S21), suggesting the films were robust to form free-standing networks. The above results indicate that our strategy is applicable to various monophenol-containing molecules and can be used to coat diverse substrates with well-connected networks. That is, enzyme-mediated assembly endows monophenol-containing building blocks with the multiple benefits (e.g., universal adhesion) of catechol-based films.

Next, the functionality of the building blocks after conversion by tyrosinase and incorporation into films was explored. The trypsin′–iron particles were enzymatically active, as evidenced by their ability to convert N_α-benzoyl-DL-arginine *p*-nitroanilide (a substrate of trypsin) into a chromophoric species (Figure S22).[28] Approximately 80% of the trypsin enzymatic activity was maintained after incorporation into the films (Figure S23). Moreover, the thermal stability of the enzymatic activity was enhanced by surface conjugation compared with that of free trypsin. The trypsin′–iron coating maintained >50% of its initial activity after incubation for 30 min at 70 °C, whereas free trypsin retained only ~20% of its initial activity after incubation (Figure S24). Finally, we demonstrate that the iron-based conjugated proteins (i.e., trypsin′) have negligible cytotoxicity to MDA-MB-231 cells (Figure S25). We note, however, that some metal ions in coatings may limit their biological application because of potential toxicity to cells.[12]

Importantly, the diverse building blocks applicable to enzyme-mediated assembly have various functional groups (e.g., catechol, amino, and thiol), which are useful for secondary, surface-confined reactions to further tailor the surface properties (Figure 4a).[29] For example, owing to the metal-chelating ability of the catechol moieties, trypsin′–iron coatings could mediate the formation of metal oxides, such as nanostructured FeOOH, on the coatings through a biomineralization process. The resulting FeOOH nanorods (Figure 4b) can be used as a highly effective photocatalyst for dye degradation under visible light irradiation in the presence of H_2O_2.[30] As shown in Figure 4c, the blue color of the methyl blue solution gradually faded upon treatment with the photocatalytic trypsin′–iron coatings, and after 6 h, more than 75% of the dye was degraded under visible light irradiation . Besides metal oxides, diverse metal ions can be incorporated into the coatings, e.g., Cu and Al ions (Figure 4d,e) to form multimetal–protein coatings. Such coatings have diverse applications in biological imaging such as positron emission tomography.[31] Additionally, *N*-hydoxysuccinimide (NHS)-containing molecules can be conjugated to the coatings through

the amine groups of trypsin′ (Figure 4f,g). Specifically, Alexa Fluor™ 488 or 633 NHS ester could react with the trypsin′–iron coatings, yielding particles with green and red fluorescence under confocal laser scanning

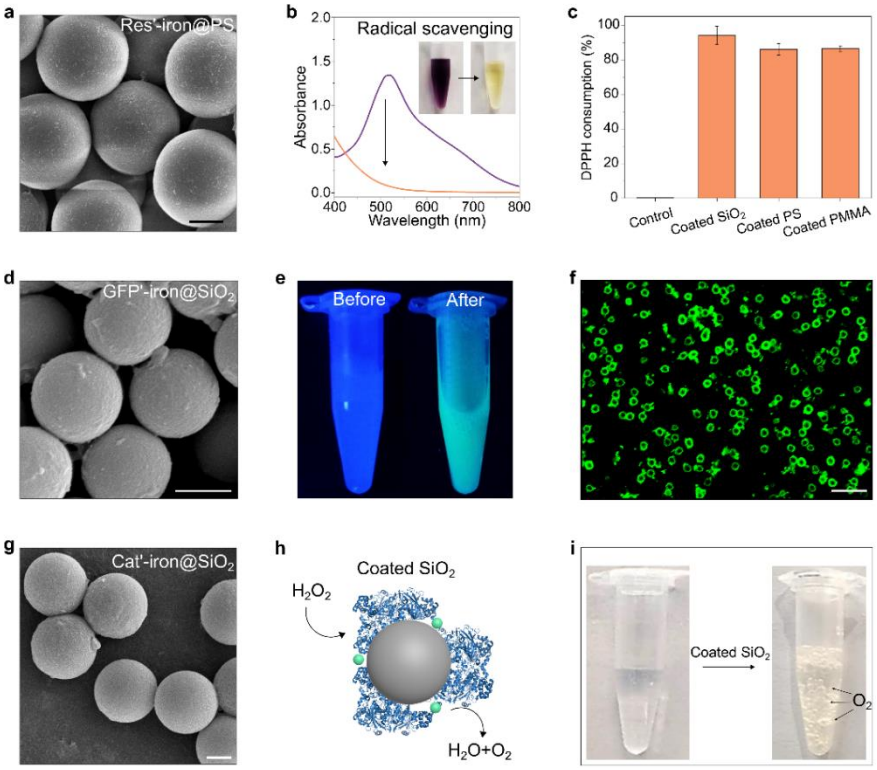

Figure 5. Potential applications of the enzyme-mediated coatings. (a) SEM image of Res′–iron@PS particles. Scale bar, 1 μm. (b) UV–vis spectra of DPPH solutions before and after treatment with Res′–iron@SiO_2 particles. Inset images show the color of the DPPH solution before and after treatment. (c) Consumption of DPPH in solutions containing different particles coated with Res′. Bare SiO_2 particles were used as a control. (d) SEM image of GFP′–iron@SiO_2 particles. Scale bar, 1 μm. (e) Photographs of SiO_2 particle suspensions before and after GFP coating under UV light irradiation. (f) CLSM image of GFP′–iron@SiO_2 particles. Scale bar, 5 μm. (g) SEM image of Cat′–iron@SiO_2 particles. Scale bar, 1 μm. (h) Schematic illustration of the decomposition of H_2O_2 to H_2O and O_2 by Cat′–iron@SiO_2 particles. (i) Photographs of H_2O_2 solutions before and after treatment with Cat′–iron@SiO_2 particles; the bubbles (O_2) generated in the tube indicate the catalytic function of the Cat′–iron@SiO_2 particles.

microscopy (CLSM), respectively. These results highlight the potential of enzyme-mediated coatings as a versatile platform for secondary, surface-confined reactions.

The well-preserved activity, universal adhesion, and biocompatibility afforded by our strategy suggest that the resulting coatings could be applicable in a wide range of applications. To demonstrate this, Res, GFP, and Cat were used to generate coatings for free radical protection, biological imaging, and catalysis, respectively (Figure 5). To demonstrate the resistance of the Res′–iron-coated particles (Res′–iron@particles) against attack from radicals, the 2,2′-diphenyl-picrylhydrazyl (DPPH) assay was used. After incubation with Res′–iron@PS particles for 30 min, DPPH solutions changed from purple to yellow, and the UV–vis absorbance at 515 nm decreased (Figure 5b), indicating the reduction of DPPH radicals.[32] Further investigation showed that 84–94% of DPPH was consumed by Res′–iron@SiO_2 particles, Res′–iron@PS particles, and Res′–iron@poly(methyl methacrylate) (PMMA) particles (Figure 5c, Figure S26), demonstrating the radical scavenging ability of the coatings on different substrates. Similarly, the GFP′–iron@SiO_2 particles showed green fluorescence (Figure 5e,f), and considering the biocompatibility of the GFP′–iron coatings (Figure S27), these particles could potentially be used for biomedical imaging. In addition, the Cat′–iron@SiO_2 particles could decompose reactive oxygen species by catalyzing H_2O_2 to H_2O and O_2, as evidenced by the generation of O_2 (Figure 5h,i). Finally, we demonstrated that a number of therapeutic biomolecules that contain monophenol groups could potentially be conjugated into MPNs by the present enzyme-mediated strategy for cancer therapies or other related biomedical applications (e.g., metastatic melanoma).[33] Moreover, diverse microbes (e.g., yeast) can naturally secrete monophenols. Thus, this strategy could also be used to assemble smart biohybrid systems.[34]

In conclusion, we have demonstrated a versatile method for engineering coatings, films, and particles from monophenol-containing molecules using enzyme-mediated assembly. Various monophenols, including small molecules (i.e., natural/synthetic monophenols) and biopolymers (i.e., synthetic polymers, peptides, and proteins), can form metal–phenolic networks on planar and particle surfaces of different size, shape, and composition. The resulting coatings can subsequently serve as a reactive platform for diverse surface-confined secondary reactions, leading to metal oxide films, multimetal–protein

coatings, and covalently conjugated films. Moreover, this coating strategy endows surfaces with various functions inherent to the original monophenol-containing building blocks, including enzymatic catalysis, radical scavenging, fluorescence, and biocompatibility. Considering the diversity of monophenol-containing molecules, the applicability of our strategy, and the capacity to tailor the surface properties, we anticipate that this enzyme-mediated assembly strategy will open up avenues for generating engineered films for a range of applications.

Acknowledgements

This research was conducted and funded by the Australian Research Council (ARC) Centre of Excellence in Convergent Bio-Nano Science and Technology (project number CE140100036) and the ARC through a Discovery Project Scheme (DP170103331). F.C. acknowledges the award of a National Health and Medical Research Council Senior Principal Research Fellowship (GNT1135806). We thank Yutian Ma and Marcin Wojnilowicz (The University of Melbourne) for helpful discussions.

Keywords: surface modification, polyphenols, metal–organic films, thin films, self-assembly

[1] a) G. Decher, *Science* **1997**, *277*, 1232–1237; b) F. Caruso, R. A. Caruso, H. Möhwald, *Science* **1998**, *282*, 1111–1114; c) D. Y. Ryu, K. Shin, E. Drockenmuller, C. J. Hawker, T. P. Russell, *Science* **2005**, *308*, 236–239; d) J. C. Love, L. A. Estroff, J. K. Kriebel, R. G. Nuzzo, G. M. Whitesides, *Chem. Rev.* **2005**, *105*, 1103–1169; e) J. J. Richardson, M. Björnmalm, F. Caruso, *Science* **2015**, *348*, aaa2491; f) S. Ma, C. Yan, M. Cai, J. Yang, X. Wang, F. Zhou, W. Liu, *Adv. Mater.* **2018**, *30*, 1803371; g) R. Liu, J. Zhao, Q. Han, X. Hu, D. Wang, X. Zhang, P. Yang, *Adv. Mater.* **2018**, *30*, 1802851; h) J. Kobayashi, T. Okano, Bull. *Chem. Soc. Jpn.* **2019**, *92*, 817–824; i) K. Ariga, E. Ahn, M. Park, B.-S. Kim, *Chem. Asia J.* **2019**, *14*, 2553–2566.

[2] a) K. Lan, Y. Xia, R. Wang, Z. Zhao, W. Zhang, X. Zhang, A. Elzatahry, D. Zhao, *Matter* **2019**, *1*, 527–538; b) B. Su, Y. Tian, L. Jiang, *J. Am. Chem. Soc.* **2016**, *138*, 1727–1748; c) S. Gao, J. Hou, Z. Deng, T. Wang, S. Beyer, A. G. Buzanich, J. J. Richardson, A. Rawal, R. Seidel, M. Y. Zulkifli, W. Li, T. D. Bennett, A. K. Cheetham, K. Liang, V. Chen, *Chem* **2019**, *5*, 1597–1608.

[3] M. Abbas, Q. Zou, S. Li, X. Yan, *Adv. Mater.* **2017**, *29*, 1605021.

[4] X. Lian, Y. Fang, E. Joseph, Q. Wang, J. Li, S. Banerjee, C. Lollar, X. Wang, H. C. Zhou, *Chem. Soc. Rev.* **2017**, *46*, 3386–3401.

[5] M. A. Boles, D. Ling, T. Hyeon, D. V. Talapin, *Nat. Mater.* **2016**, *15*, 141–153.

[6] R. Qin, Y. Liu, F. Tao, C. Li, W. Cao, P. Yang, *Adv. Mater.* **2019**, *31*, 1803377.

[7] a) H. A. Lee, Y. Ma, F. Zhou, S. Hong, H. Lee, *Acc. Chem. Res.* **2019**, *52*, 704–713; b) M. A. Rahim, S. L. Kristufek, S. Pan, J. J. Richardson, F. Caruso, *Angew. Chem. Int. Ed.* **2019**, *58*, 1904–1927; *Angew. Chem.* **2019**, *131*, 1920–194.

[8] a) Q. Z. Zhong, S. Li, J. Chen, K. Xie, S. Pan, J. J. Richardson, F. Caruso, *Angew. Chem. Int. Ed.* **2019**, *58*, 12563-12568; *Angew. Chem.* **2019**, *131*, 12693–12698; b) Z. Wang, H. C. Yang, F. He, S. Peng, Y. Li, L. Shao, S. B. Darling, *Matter* **2019**, *1*, 115–155.

[9] K. Liang, J. E. Chung, S. J. Gao, N. Yongvongsoontorn, M. Kurisawa, *Adv. Mater.* **2018**, *30*, 1706963.

[10] Y. Wang, J. P. Park, S. H. Hong, H. Lee, *Adv. Mater.* **2016**, *28*, 9961–9968.

[11] H. Lee, S. M. Dellatore, W. M. Miller, P. B. Messersmith, *Science* **2007**, *318*, 426–430.

[12] H. Ejima, J. J. Richardson, K. Liang, J. P. Best, M. P. van Koeverden, G. K. Such, J. Cui, F. Caruso, *Science* **2013**, *341*, 154–157.

[13] Q. Ye, F. Zhou, W. Liu, *Chem. Soc. Rev.* **2011**, *40*, 4244–4258.

[14] a) H. Lee, B. P. Lee, P. B. Messersmith, *Nature* **2007**, *448*, 338–341; b) C. R. Matos-Pérez, J. D. White, J. J. Wilker, *J. Am. Chem. Soc.* **2012**, *134*, 9498–9505; c) J. Yu, Y. Kan, M. Rapp, E. Danner, W. Wei, S. Das, D. R. Miller, Y. Chen, J. H. Waite, J. N. Israelachvili, *Proc. Natl. Acad. Sci. U.S.A.* **2013**, *110*, 15680–15685; d) G. P. Maier, M. V. Rapp, J. H. Waite, J. N. Israelachvili, A. Butler, *Science* **2015**, *349*, 628–632; e) J. Guo, B. L. Tardy, A. J. Christofferson, Y. Dai, J. J. Richardson, W. Zhu, M. Hu, Y. Ju, J. Cui, R. R. Dagastine, I. Yarovsky, F. Caruso, *Nat. Nanotechnol.* **2016**, *11*, 1105–1111.

[15] a) T. S. Sileika, D. G. Barrett, R. Zhang, K. H. A. Lau, P. B. Messersmith, *Angew. Chem. Int. Ed.* **2013**, *52*, 10766–10770; *Angew. Chem.* **2013**, *125*, 10966–10970; b) D. G. Barrett, T. S. Sileika, P. B. Messersmith, *Chem. Commun.* **2014**, *50*, 7265-7268; c) M. A. Rahim, K. Kempe, M. Müllner, H. Ejima, Y. Ju, M. P. van Koeverden, T. Suma, J. A. Braunger, M. G. Leeming, B. F. Abrahams, F. Caruso, *Chem. Mater.* **2015**, *27*, 5825–5832.

[16] S. Quideau, D. Deffieux, C. Douat-Casassus, L. Pouysegu, *Angew. Chem. Int. Ed.* **2011**, *50*, 586–624; *Angew. Chem.* **2011**, *123*, 610–646.

[17] A. Korner, J. Pawelek, *Science* **1982**, *217*, 1163–1165.

[18] J. Y. Kim, W. I. Kim, W. Youn, J. Seo, B. J. Kim, J. K. Lee, I. S. Choi, *Nanoscale* **2018**, *10*, 13351–13355.

[19] H. Lee, W. I. Kim, W. Youn, T. Park, S. Lee, T. S. Kim, J. F. Mano, I. S. Choi, *Adv. Mater.* **2018**, *30*, 1805091.

[20] N. R. Perron, H. C. Wang, S. N. DeGuire, M. Jenkins, M. Lawson, J. L. Brumaghim, *Dalton Trans.* **2010**, *39*, 9982–9987.

[21] M. J. Sever, J. T. Weisser, J. Monahan, S. Srinivasan, J. J. Wilker, *Angew. Chem. Int. Ed.* **2004**, *43*, 448-450; *Angew. Chem.* **2004**, *116*, 454–456.

[22] Q. Wu, Z. Xu, Y. Duan, Y. Zhu, M. Ou, X. Xu, *RSC Adv.* **2017**, *7*, 28114–28123.

[23] a) F. Ponzio, J. Barthès, J. Bour, M. Michel, P. Bertani, J. Hemmerlé, M. d'Ischia, V. Ball, *Chem. Mater.* **2016**, *28*, 4697–4705; b) X. Du, L. Li, J. Li, C. Yang, N. Frenkel, A. Welle, S. Heissler, A. Nefedov, M. Grunze, P. A. Levkin, *Adv. Mater.* **2014**, *26*, 8029–8033.

[24] W. Yang, C. Liu, Y. Chen, *Langmuir* **2018**, *34*, 3565–3571.

[25] J. R. Ros, J. N. Rodríguez-López, F. García-Cánovas, *Biochim. Biophys. Acta* **1993**, *1163*, 303–308.

[26] a) C. Maerten, L. Lopez, P. Lupattelli, G. Rydzek, S. Pronkin, P. Schaaf, L. Jierry, F. Boulmedais, *Chem. Mater.* **2017**, *29*, 9668–9679; b) S. Kim, A. M. Peterson, N. Holten-Andersen, *Chem. Mater.* **2018**, *30*, 3648–3655.

[27] B. Yang, C. Lim, D. S. Hwang, H. J. Cha, *Chem. Mater.* **2016**, *28*, 7982–7989.

[28] H. He, S. Averick, P. Mandal, H. Ding, S. Li, J. Gelb, N. Kotwal, A. Merkle, S. Litster, K. Matyjaszewski, *Adv. Sci.* **2015**, *2*, 1500069.

[29] a) Q. Z. Zhong, M. H. Yi, Y. Du, A. He, Z. K. Xu, L. S. Wan, *Adv. Mater. Interfaces* **2017**, *4*, 1700490; b) S. M. Kang, N. S. Hwang, J. Yeom, S. Y. Park, P. B. Messersmith, I. S. Choi, R. Langer, D. F. Anderson, H. Lee, *Adv. Funct. Mater.* **2012**, *22*, 2949–2955; c) Q. Wei, R. Haag, *Mater. Horiz.* **2015**, *2*, 567–577.

[30] B. Wang, H. Wu, L. Yu, R. Xu, T. T. Lim, X. W. Lou, *Adv. Mater.* **2012**, *24*, 1111–1116.

[31] J. Guo, Y. Ping, H. Ejima, K. Alt, M. Meissner, J. J. Richardson, Y. Yan, K. Peter, D. von Elverfeldt, C. E. Hagemeyer, F. Caruso, *Angew. Chem. Int. Ed.* **2014**, *53*, 5546–5551; *Angew. Chem.* **2014**, *126*, 5652–5657.

[32] G. Lin, M. A. Rahim, M. G. Leeming, C. Cortez-Jugo, Q. A. Besford, Y. Ju, Q. Z. Zhong, S. T. Johnston, J. Zhou, F. Caruso, *ACS Appl. Mater. Interfaces* **2019**, *11*, 17714–17721.

[33] K. Li, J. J. Richardson, B. L. Tardy, H. Ejima, W. Huang, J. Guo, X. Liao, B. Shi, *Adv. Sci*. **2019**, *6*, 1801688.
[34] J. Guo, M. Suástegu, K. K. Sakimoto, V. M. Moody, G. Xiao, D. G. Nocera, N. S. Joshi, *Science* **2018**, *362*, 813–816.

Entry for the Table of Contents

COMMUNICATION

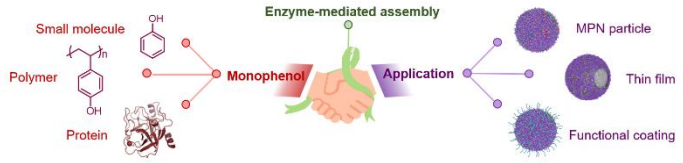

The **toolbox of metal–phenolic** networks is expanded by enzyme-mediated assembly, where a range of monophenols (14 molecules studied herein) are converted into catechol-containing molecules and cross-linked by metal ions. This strategy preserves functionality of the monophenol precursors, while conferring benefits of catechol-containing molecules (e.g., universal adhesion) to the networks.

*Qi-Zhi Zhong, Joseph J. Richardson, Shiyao Li, Wenjie Zhang, Yi Ju, Jianhua Li, Shuaijun Pan, Jingqu Chen, and Frank Caruso**

Page No. – Page No.

Expanding the Toolbox of Metal–Phenolic Networks via Enzyme-Mediated Assembly